Highly miniaturized laser ablation time-of-flight mass spectrometer for a planetary rover

Urs Rohner,[a] James A. Whitby, and Peter Wurz
Physikalisches Institut, University of Bern, CH-3012 Bern, Switzerland

Stas Barabash
Swedish Institute of Space Physics (IRF), SE-981 28 Kiruna, Sweden

(Received 10 November 2003; accepted 10 February 2004; published 26 April 2004)

We report the development and testing of a highly miniaturized mass spectrometer and ion source intended to be deployed on an airless planetary surface to measure the elemental and isotopic composition of solids, e.g., rocks and soils. Our design concentrates at this stage on the proposed BepiColombo mission to the planet Mercury. The mass analyzer is a novel combination of an electrostatic analyzer and a reflectron time-of-flight design. The ion source utilizes a laser induced plasma, which is directly coupled into the mass analyzer. Laser ablation gives high spatial resolution and avoids the need for sample preparation. Our prototype instrument has a demonstrated mass resolution $m/\Delta m$ full width at half maximum in excess of 180 and a predicted dynamic range of better than five orders of magnitude. We estimate that a flight instrument would have a mass of 280 g (including laser and all electronics), a volume of 84 cm^3, and could operate on 3 W power.
 [DOI: 10.1063/1.1711152]

I. INTRODUCTION

The European Space Agency (ESA) is studying at the moment various planetary missions, including the ''Cornerstone'' mission BepiColombo to Mercury, and the ''Flagship'' ExoMars mission to Mars. Within both these missions, it was planned to include a lander and/or rover that will investigate the composition and properties of the surface at selected locations.[1,2] The instruments on lander and rover would provide both ''ground-truth'' for the composition instruments on the orbiting spacecraft, and allow a higher resolution and more detailed analyzis of the Hermean regolith in the vicinity of the landing site. Knowledge of the composition of the crust of Mercury would allow us to estimate the composition of the planet's interior, to distinguish between models of formation, and also to develop an understanding of the relevant geochemical differentiation processes.

In order to obtain appropriate measurements of the crust we have developed a laboratory prototype of a mass spectrometer that could be incorporated into a rover of the small size envisaged for the Mercury mission. A mass spectrometer is appropriate for such a mission because a single instrument will allow the measurement of both elemental and isotopic compositions with a spatial resolution (lateral and vertical) better than the expected regolith grain size, thus allowing an accurate picture of the modal mineralogy to be built up. The high spatial resolution is of key importance as it will permit a detailed assessment of the individual constituents of the regolith and the significance of particular analyzes to the global picture. It has been suggested, for example, that Mercury's surface may contain a significant component of meteoritic origin[3] and that, as on the Moon, agglutinates and glass will form a significant fraction of surface material.[4]

The mass and power constraints for the proposed Mercury lander are severe—approximately 7 kg for the scientific payload and just 400 W h energy for both the rover and its scientific payload.[1] For the rover a scientific payload of less than 1 kg and a maximum power of 5 W are anticipated, so any instrument must be very economical in its use of these resources. The environmental conditions on Mercury are extreme with a surface temperature of up to +470 °C on the day side and −180 °C on the night side. The preferred landing place is on the cold side with the possibility of temperature control using heat dissipated by the instrument electronics. Furthermore, an air-bag landing will be used resulting in shock loads of up to 200 g. Because of these challenging conditions, we expect that an instrument designed for Mercury could be used on other (airless) planetary surfaces with little or no modification.

II. DESIGN

The design of this spectrometer is based on the experience gained from a previous larger prototype,[5] which was designed for the landing unit itself. There we already used direct laser ablation of the surface, producing a plasma plume which can be coupled directly into a mass analyzer. This technique allows a simple introduction of solid samples into a mass spectrometer (MS), whereas other techniques require preprocessing and preparation of the material to be analyzed, e.g., acid dissolution for inductively coupled plasma (ICP)–MS, embedding in a conducting material for glow-discharge or spark-source mass spectrometry.[6] Although the laser ablation ionization technique and the resulting large energy spread of the ions produced may result in elemental and isotopic fractionation effects, these can be minimized by careful control of operating parameters, and by

[a]Electronic mail: urs.rohner@phim.unibe.ch

the calibration of matrix effects. A natural choice for a mass analyzer to use with a laser ablation ion source is a time-of-flight (TOF) instrument. TOFs are robust, allow ion-optical correction of the large kinetic energy spread of ablated ions, make optimum use of a pulsed source with a low duty cycle, and are fast at acquiring spectra (typically a few microseconds for one spectrum and a few seconds for one measurement consisting of several thousand averaged spectra). Furthermore, we are able to capitalise upon our experience of building the RTOF instrument on the ROSETTA comet rendezvous mission[7] by essentially miniaturizing the existing mass analyzer.

A. Laser ablation ion source

Several publications have shown that the laser irradiance on the target must be of the order of 1 GW cm^{-2} to produce a plasma plume with minimal elemental fractionation relative to the true composition of the surface.[8–10] To produce this high irradiance from a compact solid state laser requires a short-pulse Q-switched system, which is also advantageous for coupling with a time-of-flight mass analyzer. For a miniature mass analyzer with flight times of about 5 μs, a temporal ion pulse width at the detector of 10 ns is required for a mass resolution of 250. Therefore, in practice the laser pulse width at the start should be of the order of 1 ns. The laser wavelength is expected to be less important than irradiance or pulse length, but the physical properties of the laser-induced plasma do depend on all these parameters to some extent.[8]

The low mass and power budgets of an interplanetary mission, and the severe shock loads associated with the rocket launch and planetary landing lead naturally to the choice of a diode-pumped passively Q-switched microchip laser; these devices have been described in detail elsewhere.[11] Their suitability for this application stems principally from their small size, the monolithic nature of the laser cavity [in this case mirrors are coated onto the ends of a Nd:yttrium–aluminum–garnet (YAG) gain medium and Cr:YAG Q-switch which together form a single crystal], and the simplicity of passive Q-switching (no extra components or control circuitry). Additional advantages include good beam quality (allowing the laser beam to be focused to a small spot, or readily frequency doubled) and the fact that output pulse energy is approximately independent of the pump power.

In this work we report results obtained using either green laser light at 532 nm or infrared laser light at 1064 nm. Both systems were obtained from Northrop Grumman Space Technology-Synoptics. The 532 nm MegaChip device (ML-00039) produces 4 μJ pulses at 7 kHz with a pulse width of 0.66 ns, whereas the 1064 nm MegaChip device (ML-00040) produces 12 μJ pulses at 7 kHz with the same pulse width of 0.66 ns. The laser was focused obliquely onto the target using a 25.4 mm focal length doublet lens (Newport PAC016) after 5 cm of free propagation to produce slightly elliptical spots of approximately 15 μm diameter. The placement of the focusing lens can be seen in Fig. 1, the microchip laser is shown in the inset of Fig. 2. Figure 2 also shows the capability of depth profiling: single laser shots give shallow craters, more shots, where the sample was not moved, give deep holes. There is some evidence of melting at the edges of the holes, suggesting that the irradiance and/or beam shape could be improved. (The lasers used have a nearly Gaussian spatial profile, which results in the periphery of the focused spot always having an irradiance below that required for ablation.) The laser systems and heat sinks were housed within the same vacuum system as the mass spectrometer and were subject to standard bakeout conditions.

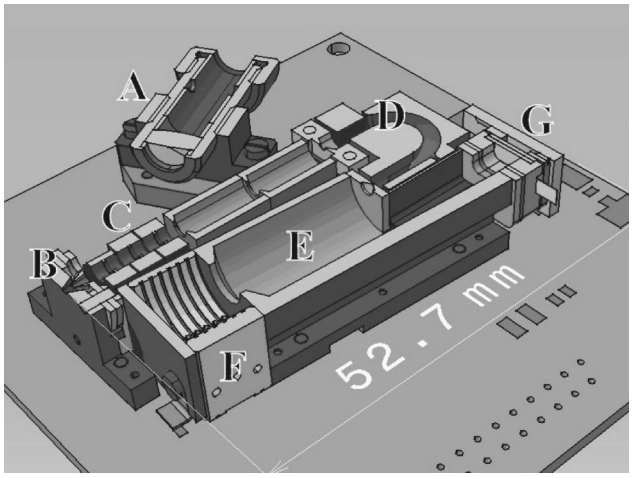

FIG. 1. Cut-away engineering drawing showing the interior of the laser mass spectrometer (LMS v2.0). (a) Laser focusing doublet lens, (b) ionization region and acceleration, (c) modified Einzel–lens, (d) electrostatic analyzer, (e) field-free drift region, (f) reflectron, and (g) MCP detector.

B. Mass analyzer

As a boundary condition for the design of the mass analyzer, ion-optic voltages were kept below 600 V, except at the detector. This was chosen to reduce the complexity of the power supplies required and to allow the construction of small structures using standard mechanical techniques without having difficulties with electrical resistances or discharge effects at higher pressures. Another severe constraint on the

FIG. 2. (a) Microchip laser system in a TO-3 package with housing removed. This is a commercially available passively Q-switched laser operating at 532 nm (Synoptics ML-00039). (b) Craters from laser shots into a piece of aluminum moved across the focus of the laser beam. (c) Magnified image showing a laser-drilled hole with a diameter of about 15 μm.

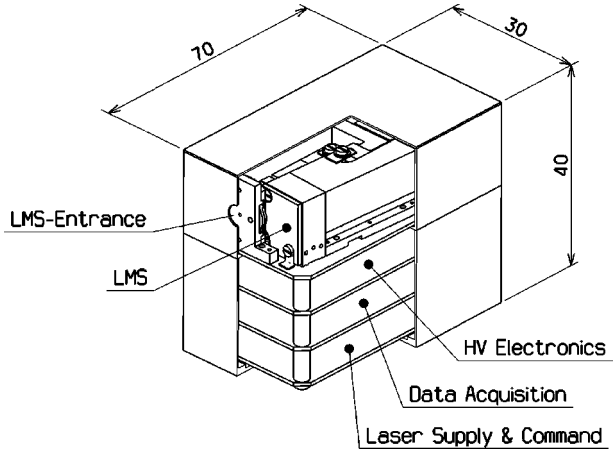

FIG. 3. A detailed engineering study of the flight version of the laser mass spectrometer (LMS) so that it can be placed on a rover (dimensions in mm). The size of the mass spectrometer corresponds to our laboratory prototype (see Fig. 5).

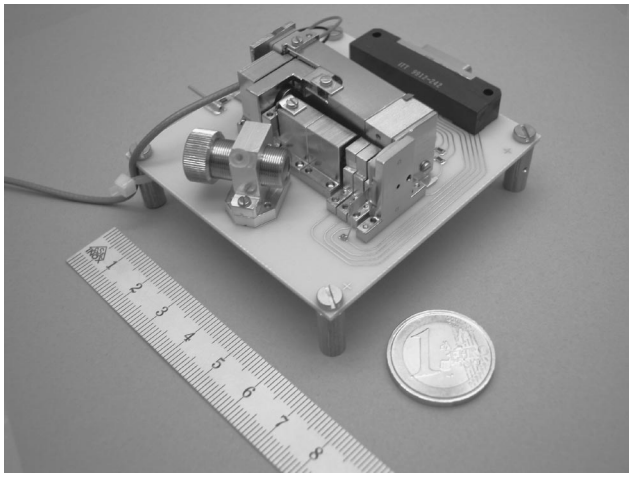

FIG. 5. Our laboratory prototype of a cigarette-box sized laser mass spectrometer (LMS) (version 2.0). The oversized power connector, lens holder, and mounting board would be eliminated for a flight version. The ruler scale is in centimeters.

design was the small volume available within the proposed rover—just 7 cm by 3 cm by 4 cm for each scientific instrument. Figure 3 shows how the mass spectrometer together with its electronics will be accommodated into a payload compartment. The compartment is so small that a simple miniaturization of our earlier axial ion-optical design[5] was not possible. For this reason, we chose a nonaxial design with a unique combination of both an electrostatic analyzer and a reflectron. Figure 1 shows an engineering drawing of the interior of the mass spectrometer.

Positively charged ions produced at the entrance are accelerated towards the Einzel-lens and focused onto the entrance of the electrostatic analyzer (ESA). Between the Einzel-lens and the ESA the ions are in a field-free region. The electrostatic analyzer acts as a shaped ion-optical mirror to guide the ions into the reflectron. However, the ESA not only focuses the transmitted ions in space and time,[12] but also acts as an energy bandpass filter for the ions passing through it. The reflectron is built as a grid-free ion mirror with seven metal rings and the backplate at separate electrical potentials. The reflectron acts to time focus the ions at the detector. The detector, which is shown in Fig. 4, consists of two chevron-mounted microchannel plates and an impedance matched anode, which is essentially a miniaturized version of the detector described in Ref. 13. The active area of the detector is 4×4 mm, necessitating specially cut microchannel plates (MCPs). By varying the voltages in the reflectron, the position and orientation of the time focus (which is usually a plane perpendicular to the drift tube) can be changed. This allows the optimal usage of alternative and more robust detectors such as a channeltron or a discrete-dynode detector.

The whole mass spectrometer is built on a printed circuit board allowing the connection of ion-optical elements to their respective potentials in a very small space and the mounting of both active and passive electronic components directly onto both sides of the board. Fig. 5 shows the realized prototype instrument, which has already the final dimensions. In the present version, this printed circuit board is larger than it would be in the final, e.g., flight, configuration.

Most of the ion-optical parts are geometrically shielded or far away from the ion plume—therefore surface contamination of the ion-optical elements or insulators by ablated material can be neglected. This has been verified with our laboratory prototype, which has been exposed to much more

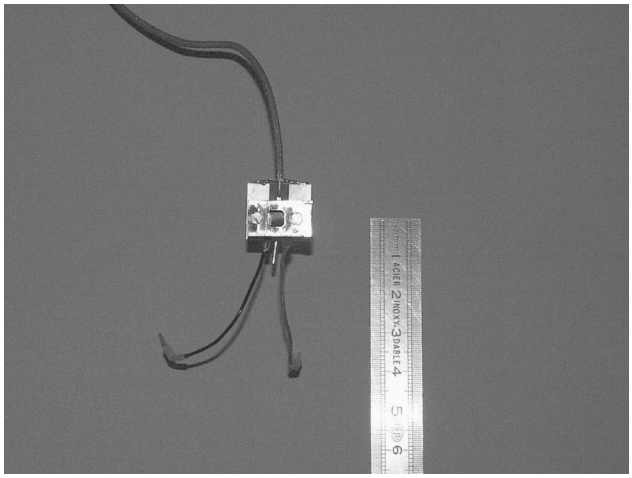

FIG. 4. Miniature microchannel plate detector with a time resolution of 0.33 ns. The two thin cables are for the power supply, the thicker one is the signal cable. The ruler scale is in centimeters.

TABLE I. Ion-plume parameter dependent mass resolution calculated from detailed simulations using SIMION v7 and 222 000 ions. An angle of 0° for σ_ρ, σ_φ implies all the ions move perpendicular to the target surface.

	Plume parameter				$m/\Delta m$ at		
	$\sigma_x, \sigma_y, \sigma_z$ (μm)	$\sigma_\rho, \sigma_\varphi$ (deg)	σ_E (eV)	Trans. (%)	50%	10%	1%
a	0.1	20	100	1.90	555	309	136
b	10	20	100	1.69	530	226	123
c	20	20	100	1.26	403	194	100
d	50	20	100	0.55	226	113	68
e	100	20	100	0.20	143	75	43
f	10	180	100	0.07	520	226	104
g	10	0	100	6.09	1015	522	208

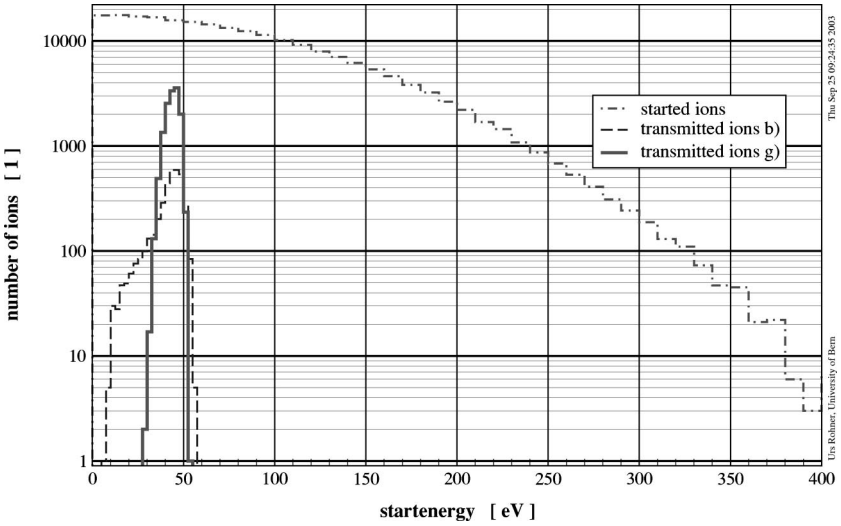

FIG. 6. Distribution of the initial energy of the ions in the ion plume with start parameters (b) and (g) of Table I.

potential contamination than we expect from a limited duration mission.

C. Ion-optical simulations

Following the initial selection of geometry and approximate dimensions, all voltages and positions of the ion-optical elements were optimised using the computer program SIMION v7[14] in conjunction with a set of macros and C-programs.[15] A merit function was constructed to optimize the transmission and mass resolution within the constraints imposed on the voltages and overall dimensions. To estimate the transmission and mass resolution obtainable, we assumed that the laser-produced plasma consists of a plume of ions (and electrons) with an initial position described by a three-dimensional Gaussian distribution with widths σ_x, σ_y, σ_z centered on the symmetry axis at the entrance of the spectrometer. The initial direction distribution of the ions was modeled as a Gaussian distribution normal to the target surface with angular widths of σ_ρ and σ_φ (ρ=azimuth angle, φ=elevation angle). The energy distribution of the ions was assumed to be a half-Gaussian with cutoff at 0 eV and an energy width of σ_E. The effects of plasma shielding were neglected entirely because with these parameters and a subnanosecond laser pulse, it is expected that the plasma jet does not travel a significant distance in the time it takes for the plasma to cool, and thus for the Debye length to become large and the plasma to become ''transparent'' to electric fields. The choice of angular and energy dispersions was guided by theoretical and measured values[8,9,16,17] and is justified by our results as described later (see Sec. III) and in Ref. 5.

Table I shows the calculated transmissions and mass resolutions for different ion-plume parameters (transmission is defined here as ion-optical transmission from the origin of the ions to the detector entrance; ionization efficiency and detector efficiency are not included). The voltage settings were automatically optimized for the ions with start parameters given in row (g) using an objective function which was a multiplication of transmission and resolution with suitable boundary conditions. In rows (a)–(e), the initial spread in the ion's start position was increased from 0.1 to 100 μm (this means in the last case that approximately 68% of the ions started in a hemispherical volume with a radius of 100 μm around the center). The resulting transmission decreases by a factor of 10, whereas the mass resolution only decreases by a factor of 4. In row (f), a (physically implausible) plume is

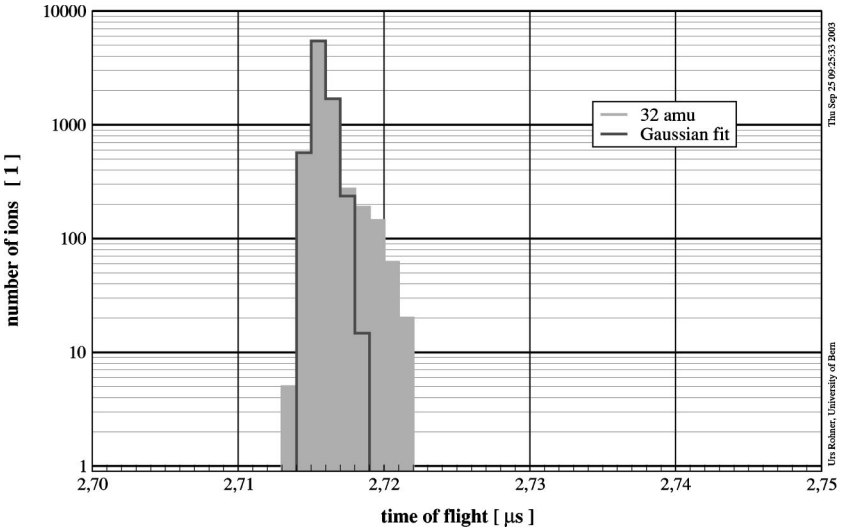

FIG. 7. Simulated mass spectrum for mass 32 with 222 000 ions using parameter set (g) of Table I. The histograming time step is 1.0 ns.

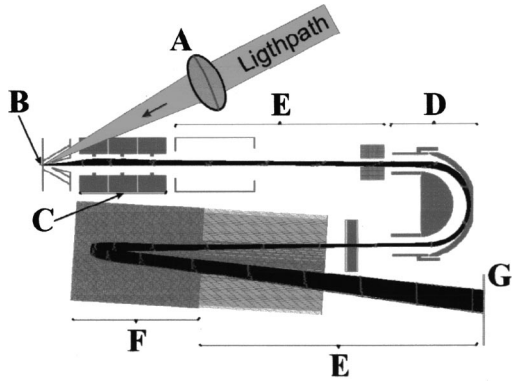

FIG. 8. Some simulated ion trajectories of ions using parameter set (b) of Table I. They are generated in point (b) and detected at the detector (g). The ion-optical elements are labeled like in Fig. 1.

shown in which most of the ions are initially traveling towards the surface and therefore only 0.07% reach the detector. In row (g), all ions are initially moving perpendicular to the target surface and towards the spectrometer. The relatively low values for the transmission are due to the wide spread of the energy distribution of the ions resulting from the laser ablation process. Figure 6 shows the energy distribution of all 222 000 simulated ions and the energy distribution of the ions with plume parameters (b) and (g), which reached the detector. In Fig. 7, a simulated mass spectrum for mass 32 is shown, using the plasma parameters (g). The next mass peak with $m/e=33$ would be well separated arriving 41 ns later than the peak with $m/e=32$. Mass resolution could be increased (at some penalty to transmission) by using additional apertures at suitable locations to remove the tail of slower ions, which are at the right side of the peak outside the Gaussian envelope. Figure 8 shows a schematic drawing of the spectrometer and some ion trajectories of ions which hit the detector (g). The ions started in point B with start parameters (b) of Table I.

D. Electronics

Due to the severe limitations in the available space and power in the proposed rover, all electronics for the mass spectrometer flight prototype had to be custom built. Power-management and laser-driver electronics, high voltage power-supplies, and data acquisition electronics have all been developed to demonstrate their sufficient miniaturization (see Figs. 3, 9, and 10).

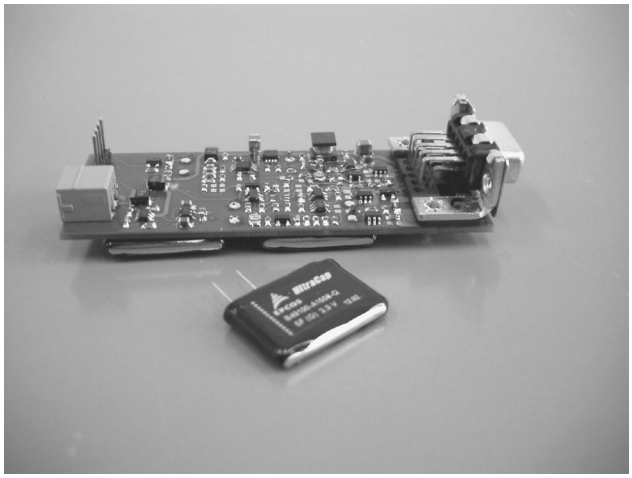

FIG. 9. Prototype laser control and power-supply electronics for the microchip laser, including temperature controller. One of the capacitors used for local energy storage is also shown in the foreground.

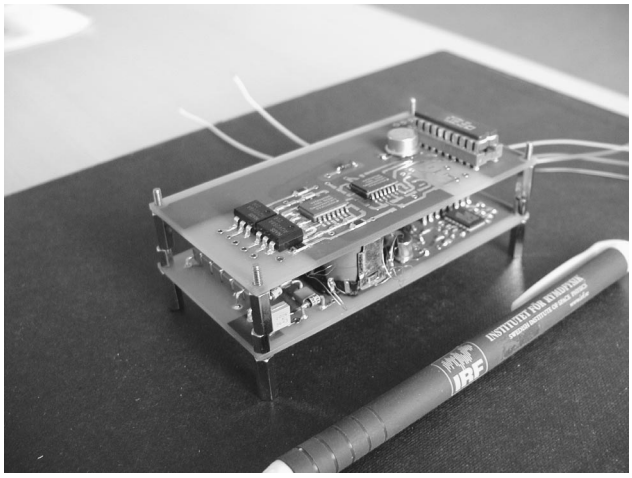

FIG. 10. Prototype high voltage electronics mounted on two boards. In future versions, the two boards will be combined in one single board using two-side mounting.

1. Laser electronics

The pump laser diode of the microchip laser needs a regulated drive current of ≈1.4 A at a voltage of 1.83 V. In addition, the diode laser needs to be operated at a fixed temperature with an accuracy of approx. ±0.5 K during one measurement time of 1–4 s for an efficient pumping of the Nd:YAG crystal. Therefore, the diode will be heated up to its operation temperature which is then regulated with a Peltier element. This element works at 1.22 V and has a temperature dependent current consumption of 0–2 A. The nominal voltage supplied by the rover for a payload instrument is 3.3 V with a maximum current of 0.8 A. To deal with the higher power and current demands of the laser system and temperature control, we make use of local energy storage in large capacitors to allow laser operation at the full repetition rate for a short time, e.g., 1–4 s. In Fig. 9, the prototype laser

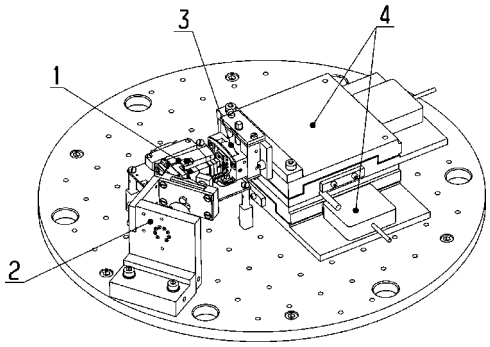

FIG. 11. Schematic view of the measurement setup in the laboratory (all in vacuum): (1) laser mass spectrometer (LMS v2.2), (2) microchip laser with holder for neutral density filters, (3) sample holder, e.g., for a 1 in. electron microprobe standard block, and (4) *xy* table.

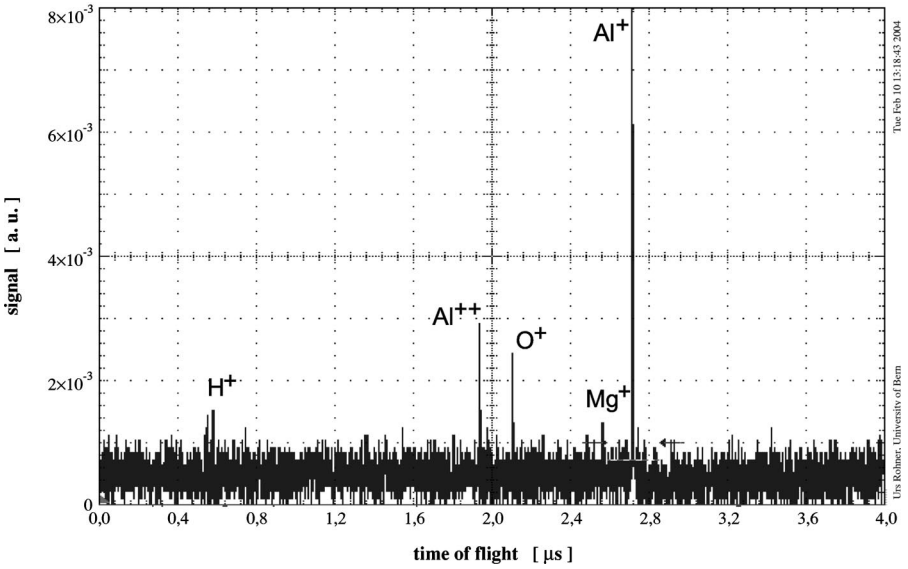

FIG. 12. Mass spectrum from a single laser shot on a aluminum alloy target (containing mainly aluminum, with small fractions of magnesium and silicon), demonstrating the single-shot mass resolution of 404 (using the 1064 nm laser).

electronics can be seen, which are in use to drive and control the microchip lasers and their peltier elements.

2. High voltage electronics

On the high voltage board, six individually controllable voltages in the range of +100 to −600 V and the detector voltage of −2.0 to −3.5 kV have to be generated. The required detector voltage depends on the type of detector used; with the microchannel-plate detector shown in Fig. 4, only −2.0 kV are needed. A single high voltage supply provides a base voltage which is serially regulated by photo metal–oxide–semiconductor relays for voltages below 1 kV and by AMPTEK HV601B optocoupler for the detector voltage. The regulation accuracy is 256 steps for each range that is sufficient for this application. The base supply in the prototype uses a common coil transformer which will be replaced by a economic flat design (EFD) one to fulfill the requirements for height. The EFD transformer has the same electrical characteristics but while slightly larger in area is two times thinner than the coil transformer. The prototype high voltage board utilized a custom-made doubler space qualified in a number of missions which will be replaced by a HM402N10 doubler from VMI Inc. if the latter can be qualified. Figure 10 shows the fully functional prototype capable of generating all voltages needed for the mass spectrometer. The prototype went successfully through thermal cycling (−40–+60 °C) meeting the specifications. Although it is at this stage made out of two stacked boards, the use of double-sided mounting and further miniaturization will eliminate one of them to give a shallow package. The constraints on length and width are already satisfied.

3. Data acquisition electronics

To record the spectra, the data acquisition electronics must digitize the detector signal for 10 μs with a time resolution of 1–5 ns to avoid degradation of the mass resolution in the sampling process. If electrical power consumption permits, it is foreseen to sample every 2.5 ns (400 Ms/s) using

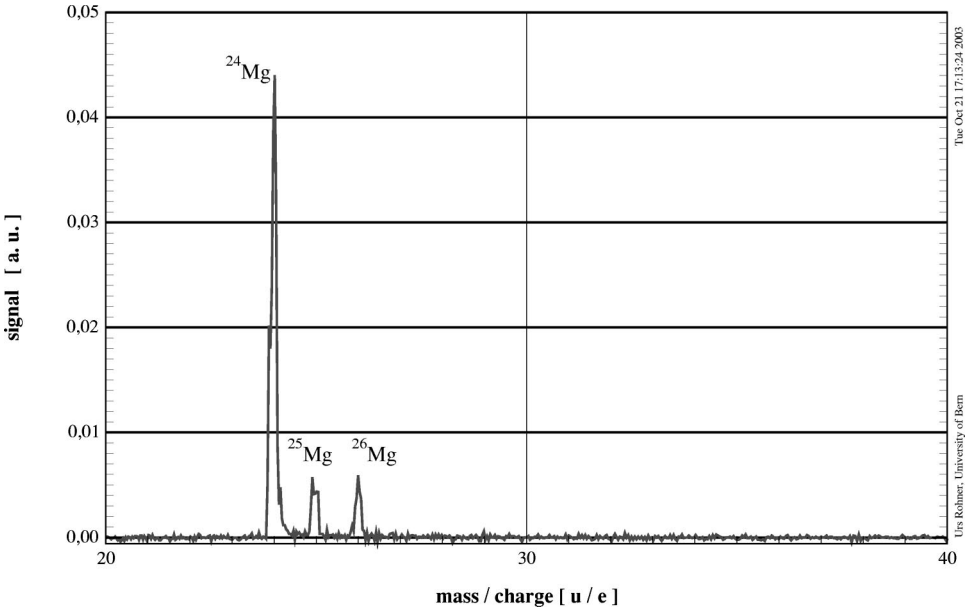

FIG. 13. Single shot mass spectrum of a magnesium target acquired with the Tektronix digital oscilloscope TDS7404 (1064 nm laser).

TABLE II. Comparison of measured and tabulated isotopic ratios of the interference-free mass peaks of the spectra shown in Figs. 13 and 14.

Sample		Measured	Standard
Mg	$^{25}Mg/^{24}Mg$	0.128	0.127
Mg	$^{26}Mg/^{24}Mg$	0.135	0.139
NBS 479	$^{53}Cr/^{52}Cr$	0.11	0.114
NBS 479	$^{57}Fe/^{56}Fe$	0.028	0.0239

4096 channels in time and 256 channels vertical (eight-bit). Otherwise, the time resolution will be scaled down to 5 ns (200 Ms/s). The overall acquisition rate of the electronics should ideally match the 7 kHz repetition rate of the free-running laser, although the possibility exists of not triggering on every laser shot in order to conserve electrical power and computional capacity. The data will be accumulated in a simple 24-bit histograming process (requiring 64 kilobytes of storage at 5 ns or 128 kByte at 2.5 ns time resolution). It is planned in the actual design to use a field programmable gate array (e.g., Actel AX500) for this purpose (if the chip can be qualified for space applications), but the data acquisition electronics are still in the design stage.

III. MEASUREMENTS

Figure 11 shows the laboratory setup used for the following measurements. The entire mass analyzer and laser system were placed in a large ultrahigh vacuum chamber that could be pumped down to 1×10^{-7} mbar. In front of the laser, there was a holder for neutral density filters to alter the laser intensity. In front of the fixed mass spectrometer was an *xy* table holding the target block which allowed samples to be changed without venting the system (and the simulation of deployment from a rover at varying positions), and also the distance between target and mass spectrometer entrance to be varied. All electronics were placed outside the vacuum chamber and electrical connections were made through high-voltage feedthroughs except for the signal from the detector which used a 50 Ω feedthrough and cable. After closing the chamber, no adjustment of the laser focus was possible except by changing the position of the sample.

For acquiring single shot spectra, an eight-bit digital oscilloscope (Tektronix TDS 7404, 4 GHz, 20 Gs/s) was used. For the acquisition of averaged spectra at the full laser repetition rate of 7 kHz, an Acquiris Averager AP200 was used. A Hamamatsu high-speed photodiode (G8376) was used for recording the laser pulse and triggering the data acquisition.

In Fig. 12 a mass spectrum from an aluminum alloy sample is shown, demonstrating the single shot mass resolution of $m/\Delta m = t/2\Delta t = 2720\ \text{ns}/2\times3.363\ \text{ns} = 404$. In this case, the 1064 nm laser was used. This represents the maximum mass resolution of the ion-optical system, which fits well with the expectations from the ion-optical simulations presented earlier. After averaging many spectra the resolution degrades since laser ablation-ionization process has fluctuations on the nanosecond time scale. The limitation of the maximum mass resolution by the detector's time resolution of 0.33 ns (full width at half maximum) pulse width for a single ion hitting the detector) is approximately $m/\Delta m = 4000$, and by the signal digitisation process with a time step of, e.g., 0.5 ns $m/\Delta m = 2700$ (both for mass 32).

Figure 13 shows a single shot mass spectrum from a pure Mg sample. The three isotopes are clearly separated (even though the mass spectrometer was not tuned to optimal performance) and even their amplitudes agree well with the tabulated isotopic abundances (see Table II). This demonstrates that the laser ionization process produces enough ions to justify data acquisition via an analog-to-digital system, rather than the simpler peak counting (time-to-digital) technique. Furthermore, we expect to increase the dynamic range from two decades for the single-shot spectrum to six decades upon signal histogramming of 10^4 spectra, e.g., data accumulation for about 1 s.

Figure 14 shows a section of a mass spectrum from a National Bureau of Standards (NBS), now National Institute of Standards and Technology steel sample (NBS 479). Again,

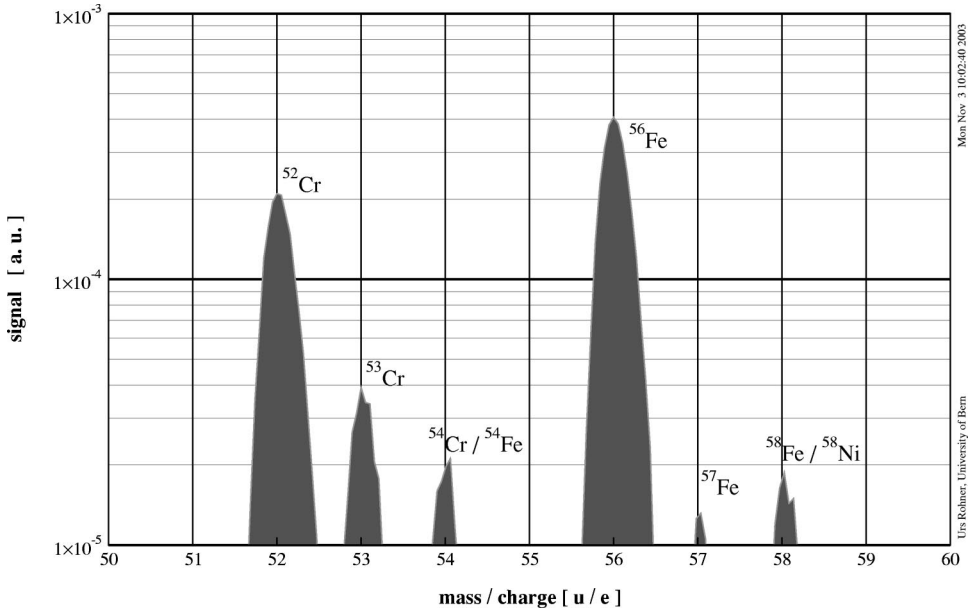

FIG. 14. Mass spectrum of a NBS steel target acquired with the Tektronix digital oscilloscope TDS7404 averaging 1800 single shot spectra (1064 nm laser on free repetition rate of 7 kHz; logarithmic scale).

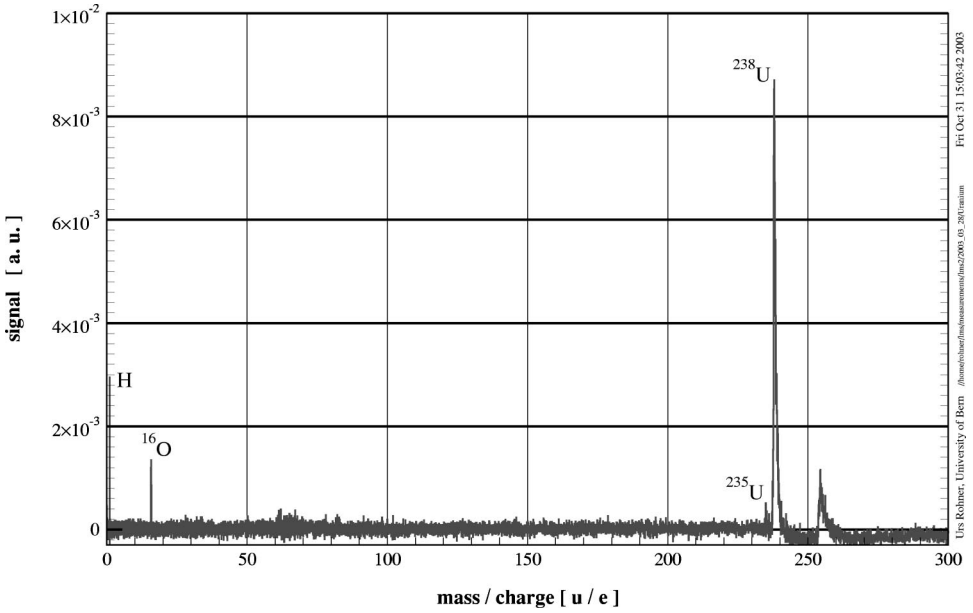

FIG. 15. Mass spectrum of a uranium target acquired with the Tektronix digital oscilloscope TDS7404 averaging approximately 200 single shot spectra (laser pulse repetition rate on 50 Hz, 1064 nm laser).

the individual isotopes of Cr, Fe, and Ni are clearly resolved, and their abundances agree well with the tabulated values (see Table II). No correction factors for isotopic instrumental mass fractionations have been applied in this analyzis. Comparison of the measured elemental abundances with the known sample composition reveals significant elemental fractionation (e.g., by the plasma ionization process) which has to be corrected with suitable calibration factors. Also inhomogeneities of the elemental composition of the NBS sample on a scale length of the laser sampling spot size ($\varnothing \approx 15\ \mu$m) cannot be excluded.

Figure 15 shows a mass spectrum of a pure uranium foil sample (natural uranium from Goodfellow with 99.98% purity) demonstrating the capability of the instrument to detect also the heavy elements. In addition to the ^{235}U mass peak, peaks are also observed due to the uranium–oxide covering the surface (and its oxygen fragment). This surface oxide signal disappears when drilling with the laser to larger depths.

IV. DISCUSSION

The results of our laboratory prototype laser mass spectrometer are very promising, with dimensions, laser source, and electronics being all plausibly ''flight-like'' in the context of ESAs BepiColombo mission to Mercury. The demonstrated mass resolution is sufficient to clearly resolve adjacent isotopes when used with laboratory data acquisition hardware. Of course, the flight data acquisition electronics will be designed to not compromise the mass resolution of the instrument. The performance of the prototype, summarized in Table III, is in good agreement with our ion-optical simulations and is more than sufficient to answer questions about the elemental and isotopic composition of Mercury's surface. For example, the present element resolution and dynamic range is superior to the performance of the famous APXS instrument of the Mars Pathfinder mission, which returned exciting data on the composition of Martian rocks and soil.[18] However, investigations to determine the optimal laser power density and the magnitude of any matrix effects are ongoing.

Based on our prototypes, we estimate that a flight version of this instrument would have a mass (without any margin) of 280 g comprised of: structure 100 g; laser control and interface electronics 50 g; high voltage power supply 80 g; and data acquisition electronics 50 g. It will consume about 3 W average power while making measurements and have a volume of 84 cm^3 including all electronics. It is anticipated that data compression and transmission will be performed by the central computer on the rover or lander.

TABLE III. Measured performance of our laboratory prototype and the expected performance for a flight model (FM).

		Measured	FM
Mass range	amu	1–300	1–300
Resolution single shot	$m/\Delta m$	400	400
Resolution multishot	$m/\Delta m$	180	300
Dynamic range single shot	1	10^2	10^2
Dynamic range multishot	1	10^4	10^6
Laser repetition rate	Hz	$1\times10^0-7\times10^3$	7×10^3
Accumulation time	s	$1\times10^{-4}-1\times10^2$	1–4

ACKNOWLEDGMENTS

The authors are grateful to W. Benz for his continuous support and J. Fischer, H. Mischler, M. Emanuelsson, and J. Jost with their teams for their contributions in the areas of design, fabrication, and electronics, respectively. This work was supported by the Swiss National Science Foundation.

[1] A. Balogh *et al.*, ESA-SCI 2000 (2000).
[2] A. Santovincenzo, CDF study report CDF-14(A) ExoMars09, Technical report, European Space Agency, 2002.
[3] M. Kueppers, The evolution of regolith in the solar system. I—The model. Icarus (in review, 2003).
[4] Y. Langevin, Planet. Space Sci. **45**, 31 (1997).
[5] U. Rohner, J. A. Whitby, and P. Wurz, Meas. Sci. Technol. **14**, 2159 (2003).

[6] J. S. Becker and H.-J. Dietze, Int. J. Mass. Spectrom. **228**, 127 (2003).
[7] M. Hohl, P. Wurz, S. Scherer, K. Altwegg, and H. Balsiger, Int. J. Mass. Spectrom. **188**, 189 (1999).
[8] C. R. Phipps and R. W. Dreyfus, *Laser Ionization Mass Analysis*, Chemical Analysis Series Vol. 124 (Wiley, New York, 1993), Chap. 4 A, pp. 369–431.
[9] H.-J. Dietze and J. S. Becker, *Laser Ionization Mass Analysis*, Chemical Analysis Series Vol. 124 (Wiley, New York, 1993), Chap. 4 C, pp. 453–504.
[10] A. K. Knight, N. L. Scherbarth, D. A. Cremers, and M. J. Ferris, Appl. Spectrosc. **54**, 331 (2000).
[11] J. J. Zayhowski, J. Alloys Compd. **303–304**, 393 (2000).
[12] W. P. Poschenrieder, Int. J. Mass Spectrom. Ion Phys. **9**, 357 (1972).
[13] R. Schletti, P. Wurz, S. Scherer, and O. H. Siegmund, Rev. Sci. Instrum. **72**, 1634 (2001).
[14] SIMION3D version 7.0, user's manual.
[15] U. Rohner, M. Wieser, and P. Wurz (unpublished).
[16] A. Vertes, P. Juhasz, M. De Wolf, and R. Gijbels, Int. J. Mass Spectrom. Ion Processes **94**, 63 (1989).
[17] R. J. De Young and W. Situ, Appl. Spectrosc. **48**, 1297 (1994).
[18] R. Rieder, T. Economou, H. Wänke, A. Turkevich, J. Crisp, J. Brückner, G. Dreibus, and H. Y. McSween, Jr., Science **278**, 1771 (1997).